united nations
educational, scientific
and cultural
organization

international atomic
energy agency

the
abdus salam
international centre for theoretical physics

SMR 1161/7

AUTUMN COLLEGE ON PLASMA PHYSICS

25 October - 19 November 1999

Self-Organized Vortical Motions Magnetized Plasmas Chapters 6 - 7

Mitsuo Kono

Chuo University
Tokyo, Japan

Chapter 6

Collective behavior of vortices in a cylindrical plasma

In this chapter collective behavior of vortices based on the modulated point vortex model is studied in a cylindrical plasma for which the diamagnetic drift direction is azimuthal and therefore vortices remain in a finite region in the course of time development. The results are compared with the observations by Antipov et al [1] and by Griffiths and Hopfinger [2].

6.1 Drift wave vortices

The Hasegawa-Mima equation in a cylindrical plasma is written as

$$\frac{\partial \Pi}{\partial t} + [\psi, \Pi] + \mathrm{v}_* \cdot \nabla \psi = 0, \tag{6.1}$$

where ψ is an electrostatic potential and

$$\Pi = \psi - \nabla^2 \psi, \tag{6.2}$$

$$\mathrm{v}_* = \frac{v_T^2}{\Omega} \mathrm{z} \times \nabla_\perp \ln n_0. \tag{6.3}$$

When the background density is assumed to be a Gaussian, $n_0 \propto exp(-r^2/r_0^2)$, then the modulated point vortex model gives a set of equations as

$$\frac{d\mathrm{r}_\alpha}{dt} = -\frac{1}{2\pi} \sum_{\beta \neq \alpha} [\kappa_\beta - v_* r_\beta^2] \frac{\mathrm{z} \times (\mathrm{r}_\alpha - \mathrm{r}_\beta)}{|\mathrm{r}_\alpha - \mathrm{r}_\beta|} K_1(|\mathrm{r}_\alpha - \mathrm{r}_\beta|), \tag{6.4}$$

where v_* is given by $v_* = v_T^2/\Omega r_0^2$, and K_1 is the modified Bessel function of the second kind.

Numerical simulations are performed to see dynamics of a cluster consisting of like-signed vortices ($\kappa_\alpha = \kappa$). In Fig.6.1 one hundred vortices distributed randomly in a rather small region at an initial moment are shown to rotate in accord around the cylinder axis and re-distribute to form an ordered state

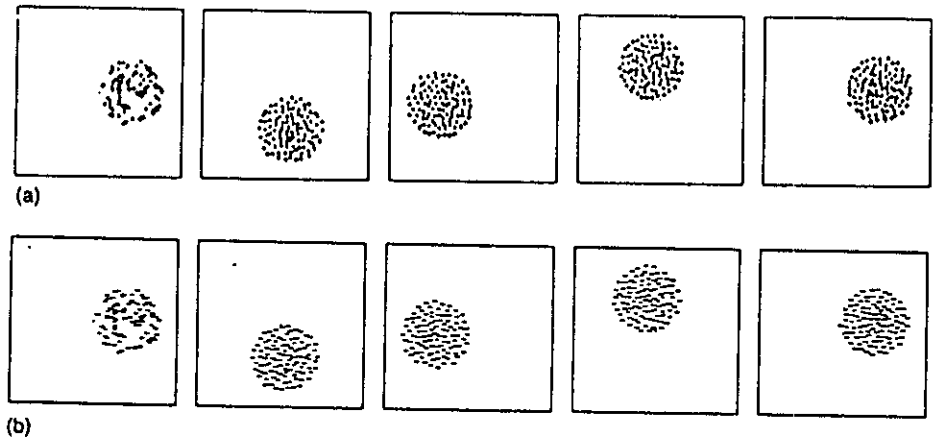

Figure 6.1: Redistribution of vortices to form an ordered state in the course of time evolution: (a) $\kappa = 100$, and (b) $\kappa = -100$, where κ is normalized by v_*.

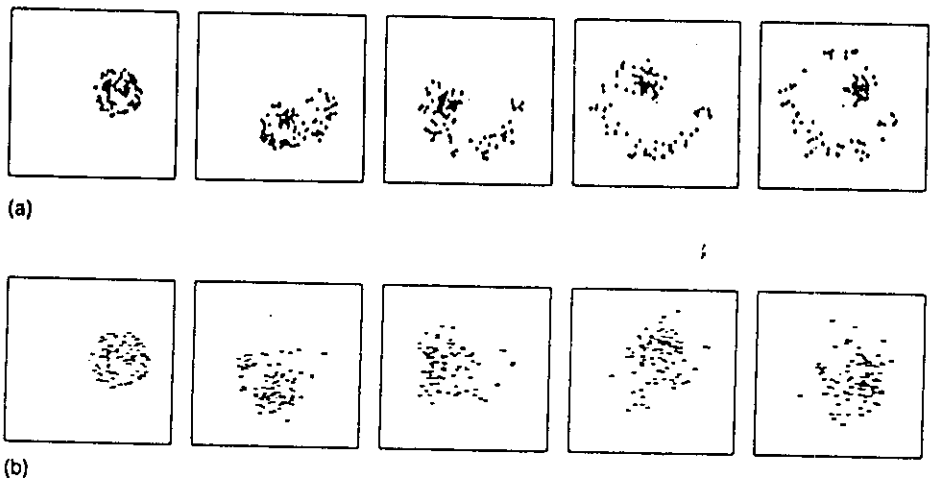

Figure 6.2: Time evolution of (a) a cyclone ($\kappa = 10$), and (b) an anticyclone ($\kappa = -10$). The κ is normalized by v_*.

inside the cluster for (a) $\kappa = 100$ and (b) $\kappa = -100$, where κ is normalized by v_*. The direction of the rotation around the cylinder axis is clockwise and does not depend on the sign of the vorticity, while the direction of the rotation inside the cluster depends on the sign of the vorticity, that is, clockwise for $\kappa > 0$ (referred to as a cyclone) and anti-clockwise for $\kappa < 0$ (referred to as an anti-cyclone). When the magnitude of κ becomes comparable to $v_* r_0$ where r_0 is a average size of the cluster, the cyclone is unstable and the outer part of the cluster is left behind the core as they rotate around the cylinder axis, while the anti-cyclone is rather stable as is shown in Fig.6.2.

Like-signed clusters collide to coalesce into one cluster when $|\kappa|$ is large and to remain themselves independent when $|\kappa|$ is not large enough (Fig.6.3). For the vortices with relatively small $|\kappa|$, only the core of two clusters with $\kappa > 0$ fuse, being undressed (Fig.6.4(a)), which can be compared with the laboratory experiments by Griffiths and Hopfinger [2] who simulated coalescence of geostrophic vortices.

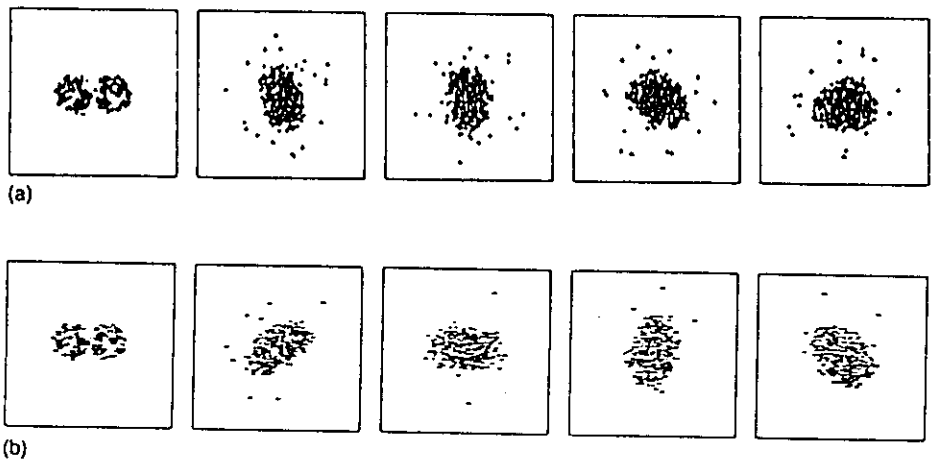

Figure 6.3: Coalescence of the like-signed clusters: (a) cyclone-cyclone ($\kappa_1 = \kappa_2 = 100$), (b) anti-cyclone-anti-cyclone ($\kappa_1 = \kappa_2 = -100$). The κ is normalized by v_*.

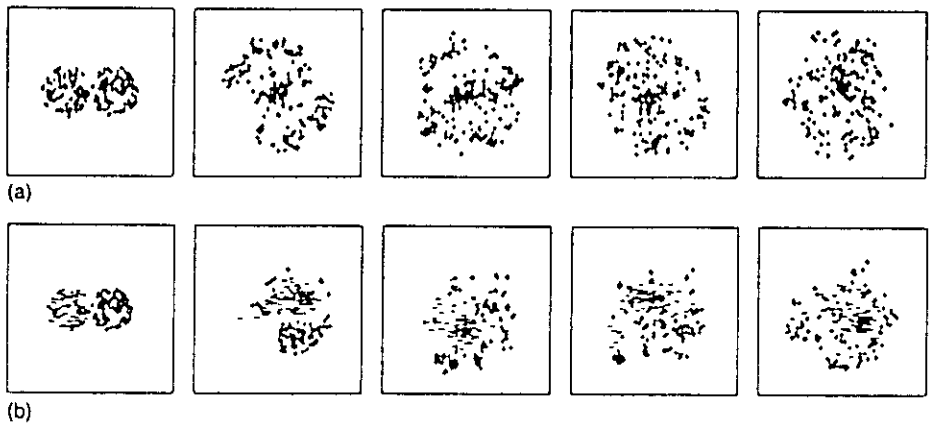

Figure 6.4: Interacting clusters with relatively small $|\kappa|$: (a) cyclone-cyclone ($\kappa_1 = \kappa_2 = 10$), and (b) cyclone-anticyclone ($\kappa_1 = -\kappa_2 = 10$).

It should be noted that coalescence of vortices has been numerically obtained by Christiansen [3] who used the cloud-in -cell (CIC) method based on the point vortex model for the Euler equation. However the CIC method inevitably introduces an effective viscosity responsible for the coalescence of the isolated vortices. On the other hand, the coalescence presented here is dynamical. While clusters with $\kappa < 0$ are inclined to coalesce into one though it takes rather long. The motion of clusters with opposite signs of κ is simply a superposition of the motion of the individual cluster (Fig.6.4(b)).

For dynamics of a cluster consisting of like-signed vortices ($\kappa_\alpha = \kappa$), denoting the coordinate of the center of mass by R and the deviation of the vortex position from it by s, that is,

$$\mathrm{r}_\alpha = \mathrm{R} + \mathrm{s}_\alpha, \quad \mathrm{R} = \frac{1}{N}\sum_\alpha \mathrm{r}_\alpha, \tag{6.5}$$

and using the identity

$$\mathbf{s}_\alpha - \mathbf{s}_\beta = \frac{\mathbf{R}\cdot(\mathbf{s}_\alpha - \mathbf{s}_\beta)}{R^2}\mathbf{R} + \frac{[\mathbf{R}\times(\mathbf{s}_\alpha - \mathbf{s}_\beta)]\times\mathbf{R}}{R^2},$$

we obtain from eq.(6.4)

$$\begin{aligned}\frac{d\mathbf{R}}{dt} &= -\frac{v_*}{4\pi N}\sum_\alpha\sum_{\beta\neq\alpha}(r_\alpha^2 - r_\beta^2)[\frac{\mathbf{R}\cdot(\mathbf{s}_\alpha-\mathbf{s}_\beta)}{R|\mathbf{s}_\alpha-\mathbf{s}_\beta|}\mathbf{z}\times\frac{\mathbf{R}}{R} + \eta_{\alpha\beta}\frac{\mathbf{R}}{R}]K_1(|\mathbf{s}_\alpha-\mathbf{s}_\beta|)\\ &\sim -\frac{v_*}{2\pi N}\mathbf{z}\times\mathbf{R}\sum_\alpha\sum_{\beta\neq\alpha}\frac{[\mathbf{R}\cdot(\mathbf{s}_\alpha-\mathbf{s}_\beta)]^2}{R^2|\mathbf{s}_\alpha-\mathbf{s}_\beta|^2}K_1(|\mathbf{s}_\alpha-\mathbf{s}_\beta|),\end{aligned} \tag{6.6}$$

where

$$\eta_{\alpha\beta} = \mathbf{z}\times\{[\mathbf{R}\times\frac{\mathbf{s}_\alpha-\mathbf{s}_\beta}{|\mathbf{s}_\alpha-\mathbf{s}_\beta|}]\times\mathbf{R}\}\cdot\frac{\mathbf{R}}{R^3}.$$

Equation (6.6) indicates that the center of mass revolves clockwise around the cylinder axis, being agitated in the radial direction. Subtracting eq.(6.6) from eq.(6.4), we have

$$\frac{d\mathbf{s}_\alpha}{dt} = -\frac{1}{2\pi}\sum_{\beta\neq\alpha}(\kappa - v_* r_\beta^2)\mathbf{z}\times\frac{\mathbf{s}_\alpha-\mathbf{s}_\beta}{|\mathbf{s}_\alpha-\mathbf{s}_\beta|}K_1(|\mathbf{s}_\alpha-\mathbf{s}_\beta|) - \frac{d\mathbf{R}}{dt}. \tag{6.7}$$

The last term on the right hand side of eq.(6.7) is neglected when $|\kappa| > v_* r_0$. For the vortices to satisfy the relation $|\mathbf{s}_\alpha - \mathbf{s}_\beta|/R << 1$, we may approximate eq.(6.7) as

$$\begin{aligned}\frac{d\mathbf{s}_\alpha}{dt} &\simeq -\frac{1}{2\pi}\sum_{\beta\neq\alpha}[\kappa - v_*(\mathbf{R}+\mathbf{s}_\beta)^2]\{\frac{\mathbf{s}_\alpha\cdot(\mathbf{s}_\alpha-\mathbf{s}_\beta)}{s_\alpha|\mathbf{s}_\alpha-\mathbf{s}_\beta|}\mathbf{z}\times\frac{\mathbf{s}_\alpha}{s_\alpha} + \varepsilon_{\alpha\beta}\frac{\mathbf{s}_\alpha}{s_\alpha}\}K_1(|\mathbf{s}_\alpha-\mathbf{s}_\beta|)\\ &\sim -\frac{1}{2\pi}[\kappa - v_*(\mathbf{R}+\mathbf{s}_\alpha)^2]\sum_{\beta\neq\alpha}\{\frac{\mathbf{s}_\alpha\cdot(\mathbf{s}_\alpha-\mathbf{s}_\beta)}{s_\alpha|\mathbf{s}_\alpha-\mathbf{s}_\beta|}\mathbf{z}\times\frac{\mathbf{s}_\alpha}{s_\alpha} + \varepsilon_{\alpha\beta}\frac{\mathbf{s}_\alpha}{s_\alpha}\}K_1(|\mathbf{s}_\alpha-\mathbf{s}_\beta|),\end{aligned} \tag{6.8}$$

where

$$\varepsilon_{\alpha\beta} = \mathbf{z}\times\{[\mathbf{s}_\alpha\times\frac{\mathbf{s}_\alpha-\mathbf{s}_\beta}{|\mathbf{s}_\alpha-\mathbf{s}_\beta|}]\times\mathbf{s}_\alpha\}\cdot\frac{\mathbf{s}_\alpha}{s_\alpha^3}.$$

From eq.(6.8) the direction of the internal rotation depends on the sign of $\kappa - v_*(\mathbf{R}+s_\alpha)^2$ since what remains of eq.(6.8) is positive definite when the vortices are distributed densely in the small region. When the sign of $\kappa - v_*(\mathbf{R}+s_\alpha)^2$ is definite during the motion, that is, κ is large enough, then the internal rotation is clockwise for $\kappa > 0$, while counterclockwise for $\kappa < 0$. For relatively large κ's , that is, $\kappa > v_*(\mathbf{R}+s_\alpha)^2$ constituent vortices redistribute themselves quite orderly as is shown in Fig.6.1. Equation (6.8) indicates that the vortices are subject to rotation for large κ and at the same time are pushed/pulled in the direction parallel to their displacements. The rotation velocity and the magnitude of the push/pull depend on the configuration of vortices. When the vortices are close each other, those rotation velocity and push/pull become large. Since the vortices are confined densely in the small region under the constraint $\sum_\alpha \mathbf{s}_\alpha = const$, they eventually redistribute themselves to separate from each other with an equal distance. This may be a mechanism behind the formation of the ordered state.

Another interesting point eq.(6.8) implies is that as $\kappa > 0$ decreases so that the sign $\kappa - v_*(\mathbf{R}+s_\alpha)^2$ changes for outer vortices, they rotate in the direction opposite to the core. Since the center of mass motion is always clockwise, the outer vortices for $\kappa > 0$ are left behind the core, while the cluster with

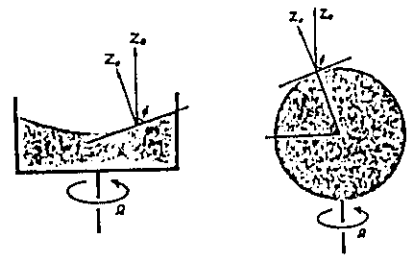

Figure 6.5: The axis along the gravitational force and the rotation axis: (a) laboratory and (b) planet

$\kappa < 0$ are absorbed into the core as is shown in Fig.6.2. Thus a cluster with $\kappa > 0$ is not long lived while a cluster with $\kappa < 0$ is long lived. These are the same at underlying physics of the observation by Antipov et al [1] who originally designed the experiment to explain the motion of drift wave vortices in an inhomogeneous magnetized plasma and the Giant Red Spot of Jupiter as well as atmospheric cyclones known as hurricanes and typhoons.

The problem is to see whether the many vortices with different polarities grow into a large vortex-pair. The vortices with the same polarity are confined in a finite region in the phase space because of the conservation law, although they exhibit complicated behaviors such as exchange scattering and mutual trapping. For the vortices with different polarities the confinement is not guaranteed by the conservation law. The repetition of the pair formation and exchange scattering seem to lead to mixing, which may not preferable to self-organization.

6.2 Monopole vortex dynamics

Since the stationary solution of the Hasegawa-Mima equation is a dipole vortex and not a monopole vortex, it has been discussed that the Hasegawa-Mima equation is not responsible for the gaint red spot of Jupiter and some other equations are needed for a monopole-like solution. One candidate discussed so far [4-6] is

$$\frac{\partial \Pi}{\partial t} + [\psi, \Pi] + \mathrm{v}_* \cdot (\mathrm{z} \times \nabla)(\psi - a\psi^2) = 0. \tag{6.9}$$

A rotating two dimensional system of shallow water with a free surface is described by the Euler equations in the geoid plane where the coordinate y is taken in a meridian direction and x is taken perpendicular to y on the geoid plane:

$$\frac{\partial}{\partial t}\mathrm{u} + (\mathrm{u} \cdot \nabla)\mathrm{u} + f\hat{\mathrm{z}} \times \mathrm{u} + g\nabla h = 0, \tag{6.10}$$

where H and h are a fluid depth in the direction of gravity and the deviation of free surface, respectively, that is,

$$H = H_0 + h(x, y, t).$$

and f is the Coriolis parameter. The continuity equation is written as

$$\frac{\partial}{\partial t}h + \nabla \cdot (H\mathbf{u}) = 0. \tag{6.11}$$

From eq.(6.10) we have

$$\begin{aligned} \mathbf{u} &= \frac{1}{f}\hat{\mathbf{z}} \times \{g\nabla h + (\mathbf{u}\cdot\nabla)\mathbf{u} + \frac{\partial}{\partial t}\mathbf{u}\} \\ &\simeq \frac{g}{f}\{\hat{\mathbf{z}} \times \nabla h - \frac{g}{f^2}[(\hat{\mathbf{z}} \times \nabla h)\cdot\nabla]\nabla h - \frac{1}{f}\frac{\partial}{\partial t}\nabla h\} \end{aligned} \tag{6.12}$$

This shows that the pressure gradient with the Coriolis force induces geophysical flow as the lowest flow. Substituting the resultant equation to eq.(6.11) gives a generalized Charney-Obukhov equation [4,5]:

$$\frac{\partial}{\partial t}(\nabla^2 h - h) + (\nabla \ln f)\cdot(\hat{\mathbf{z}} \times \nabla)(h + \frac{h^2}{2}) + [h, \nabla^2 h] = 0 \tag{6.13}$$

where h is normalized by H_0, and the space and time are normalized by the Rossby radius $r_R = \sqrt{gH_0}/f$ and the Coriolis frequency f.

The motion of 2D fluid in a magnetized plasma is described by

$$\frac{\partial n}{\partial t} + \mathbf{v}_\perp \cdot \nabla n = 0, \tag{6.14}$$

$$\mathbf{v}_\perp = \frac{c}{B_0}\mathbf{z} \times (\nabla\psi - \frac{T}{e}\nabla \ln p), \tag{6.15}$$

$$\nabla^2\psi = -4\pi e(n - n_0 e^{e\psi/T}). \tag{6.16}$$

These equations are combined to give

$$\frac{\partial}{\partial t}(\nabla^2\psi - \psi) - (\nabla \ln p)\cdot(\mathbf{z} \times \nabla)(\psi + \frac{1}{2}\phi^2) + [\psi, \nabla^2\psi] = 0, \tag{6.17}$$

where the space and time are normalized by the Debye length λ_D ($\lambda_D = T/4\pi n_0 e^2$) and $(1/\Omega)(\lambda_D/\rho)$ ($\rho = C_s/\Omega$, $C_s = T/M$, and $\Omega = eB/Mc$), respectively. An electric potential ψ is normalized by e/T and $[\ ,\ ]$ denotes a Poisson braket. Equation (6.17) is the same as is derived above for a planetary fluid and is derived by Tasso [6].

In eq.(6.17) the scalar nonlinearity $(\nabla \ln p)\cdot(\hat{\mathbf{z}} \times \nabla)\psi^2/2$ gives a solitary structure of the K-dv type (a monopole vortex) and a vector nonlinearity $[\psi, \nabla^2\psi]$ describes a dipole vortex. If the scale length of the structure is given by a, the order of magnitudes of these two terms are estimated as

$$(\nabla \ln p)\cdot(\hat{\mathbf{z}} \times \nabla)\frac{\psi^2}{2} \simeq |\nabla \ln p|\frac{\psi^2}{a},$$

$$[\psi, \nabla^2\psi] \simeq \frac{\psi^2}{a^4}$$

For a Gaussian pressure profile $p \propto exp(-r^2/2R^2)$, when the following inequality holds,

$$a > (\frac{1}{|\nabla \ln p|})^{1/3} \sim (\frac{\lambda_D^2 R^2}{a})^{1/3},$$

that is,

$$a > R\sqrt{\frac{\lambda_D}{R}}, \tag{6.18}$$

the scalar nonlinearity dominates the vector nonlinearity, indicating that the monopole type of vortices are excited.

For the planetary atomospheric motion, the Coriolis parameter is estimated in the β-plane, being expressed as

$$f = 2\Omega \sin\phi \simeq f_0 + \beta y, \quad \beta = \frac{2\Omega}{R}\cos\phi,$$

where Ω is the angular frequency of the system rotation, ϕ is the angle between the axis of the system rotation and the normal to the fluid surface and R is the diameter of the Earth. The β plane approximation is to treat the fluid rotating around the direction of gravity with the angular velocity of $2\Omega sin\phi$, for which eq.(6.18) is rewritten as

$$a < r_R(\frac{R}{r_R}\tan\phi)^{1/3}. \tag{6.19}$$

Equations (6.17) and (6.13) are intensively studied concerning the confinement and transport of magnetized plasmas and the large scale planetary atmospheric motions. So far, however, those work are rather limited to studies of nonlinear evolution of initially given monopole or dipole type of vortices, and the process in the self-organization emerged from randomly excited large number of vortices has not been studied.

The large scale motions characterized by eq.(6.18) are dominated by the monopole type of vortices for which a long wave approximation can be used to eqs.(6.17) and (6.13) to give

$$\frac{\partial}{\partial t}\psi + \mathrm{v}_* \cdot (\hat{\mathrm{z}} \times \nabla)(\psi + \nabla^2\psi + \frac{\psi^2}{2}) - [\psi, \nabla^2\psi] = 0, \tag{6.20}$$

where $\mathrm{v}_* = \nabla \ln p$ or $\nabla \ln f$, depending on which vortices are concerned.

The core part of the monopole vortex may be described by a localized function F as

$$\psi(\mathrm{r}, t) = \sum_\alpha \kappa_\alpha F_\alpha(|\mathrm{r} - \mathrm{r}_\alpha|), \tag{6.21}$$

which is substituted into eq.(6.20) to give

$$\sum_\alpha \kappa_\alpha \frac{\mathrm{r} - \mathrm{r}_\alpha}{|\mathrm{r} - \mathrm{r}_\alpha|} F'_\alpha \{-\frac{d\mathrm{r}_\alpha}{dt} + \sum_\beta \kappa_\beta \frac{\hat{\mathrm{z}} \times (\mathrm{r} - \mathrm{r}_\beta)}{|\mathrm{r} - \mathrm{r}_\beta|} F'''_\beta + \hat{\mathrm{z}} \times \mathrm{v}_*(1 + \frac{F'''_\alpha}{F'_\alpha} + \sum_\beta \kappa_\beta F_\beta)\} = 0. \tag{6.22}$$

Here the unknown function F is determined so as for the nonlinearity to balance with the dispersion, that is, the following equation holds:

$$-\lambda F'_\alpha + F'''_\alpha + \kappa_\alpha F_\alpha F'_\alpha = 0. \tag{6.23}$$

This equation is readily solved to give

$$F_\alpha(|\mathrm{r} - \mathrm{r}_\alpha|) = A_\alpha sech^2(\sqrt{\frac{\kappa_\alpha A_\alpha}{12}}|\mathrm{r} - \mathrm{r}_\alpha|), \quad A_\alpha = \frac{48\lambda}{\kappa_\alpha}, \tag{6.24}$$

where λ is a parameter to represent the spatial extent of the localized function of F. Then the motion of the center of the monopole vortex is described by

$$\frac{d\mathbf{r}_\alpha}{dt} = \sum_\beta \kappa_\beta \frac{\hat{\mathbf{z}} \times (\mathbf{r}_\alpha - \mathbf{r}_\beta)}{|\mathbf{r}_\alpha - \mathbf{r}_\beta|} F_\beta'''(|\mathbf{r}_\alpha - \mathbf{r}_\beta|) + (1 + \lambda + \sum_{\beta \neq \alpha} \kappa_\beta F_\beta(|\mathbf{r}_\alpha - \mathbf{r}_\beta|))\hat{\mathbf{z}} \times \mathbf{v}_*. \tag{6.25}$$

Here we consider the case of the like-signed vortices $\kappa_\alpha = \kappa$, and introduce the coordinate of the center of mass $\mathbf{R}$ and the deviation from it $\mathbf{s}$ as

$$\mathbf{r}_\alpha = \mathbf{R} + \mathbf{s}_\alpha, \quad \mathbf{R} = \frac{1}{N}\sum_\alpha \mathbf{r}_\alpha.$$

Then we simply have

$$\frac{d\mathbf{R}}{dt} = \mathbf{z} \times \mathbf{v}_*[1 + \lambda + \frac{1}{N}\kappa \sum_\alpha \sum_\beta F(|\mathbf{s}_\alpha - \mathbf{s}_\beta|)], \tag{6.26}$$

$$\begin{aligned} \frac{d\mathbf{s}_\alpha}{dt} &= \kappa \sum_\beta \frac{\mathbf{z} \times (\mathbf{s}_\alpha - \mathbf{s}_\beta)}{|\mathbf{s}_\alpha - \mathbf{s}_\beta|} F'''(|\mathbf{s}_\alpha - \mathbf{s}_\beta|) \\ &= \kappa \sum_\beta [\frac{\mathbf{s}_\alpha \cdot (\mathbf{s}_\alpha - \mathbf{s}_\beta)}{s_\alpha |\mathbf{s}_\alpha - \mathbf{s}_\beta|} \mathbf{z} \times \mathbf{s}_\alpha + \varepsilon_{\alpha\beta} \frac{\mathbf{s}_\alpha}{s_\alpha}] F'''(|\mathbf{s}_\alpha - \mathbf{s}_\beta|). \end{aligned} \tag{6.27}$$

The center of mass rotates in the direction of the diamagnetic drift, while the vortex positions deviated from the center of mass behave similar to those in the previous case of the drift wave vortices. Since the motion of the like-signed monopole vortices are confined in a finite region because of the constant of motion $\sum_\alpha \mathbf{s}_\alpha = const$, the vortices behave as a single large vortex which rotates in the direction of the diamagnetic drift around the cylinder axis, while the vortices are subject to rotation in accord inside the single large vortex. This could be a picture behind the Giant Red Spot in the Jupiter.

References

[1] S. V. Antipov, M. V. Nezlin, V. K. Rodrmov, A. Yu. Rylov, E. N. Snezkhin, A. S. Trubnikov and A. V. Khutoretskii, Sov. J. Plasma Phys. 14, 648 (1988)

[2] R. W. Griffiths and E. J. Hopfinger, J. Fluids Mech. 178, 73 (1987)

[3] J. P. Christiansen, J. Fluid Comput. Phys. 13, 363 (1973)

[4] J. G. Charney: On the scale of atmospheric motions, Geophys. Public. 17 , 1 (1948)

[5] A. M. Obukhov, Geografis I Geofizika 13, 281 (1949)

[6] Tasso, Phys. Letters 96A, 33 (1983)

Chapter 7

Spiral structures in magnetized rotating plasmas

Coherent structures have been recently observed in laboratories [1-5] and are subject to theoretical analysis for understanding underlying physics. In both ECR plasmas and gun-produced plasmas, two-arm spirals are commonly observed, and in particular the spiral structures observed in the ECR plasmas [4] have interesting features: (1) the stationary structure is observed in a certain range of the background pressure, (2) the direction of the arm stretching is reversed when the magnetic field is reversed, and (3) the arm winding is identified with the Archimedes spiral, that is the curve spiraling into the origin which in polar coordinates is given by the equation $r \propto \theta$.

In the ECR plasmas, the ratio of the ion collision frequency with neutral particles to the ion cyclotron frequency is small as $\nu_i/\Omega_i \sim 0.05$, and the azimuthal rotation due to the E × B drift, which is $0.2C_s \sim 0.4C_s$ (C_s: ion acoustic velocity), dominates the radial drift due to collisions. Furthermore, the ratio of the nonlinear term to the Lorenz force term $C_s/r_d\Omega_i$ is as small as ν_i/Ω_i, where r_d is the plasma radius. Thus, the radial structure of spiral formed in an azimuthally rotating plasma can be analyzed with a linear eigen-value problem. On the other hand the ratio of the electron axial drift to the electron azimuthal drift is of the order of $kr_d(\Omega_e/\nu_e)$ where k is a characteristic axial wave-number. Since Ω_e/ν_e is as large as 10^2, mode-mode coupling has to be taken into account for the fluctuations with a long wave in the axial direction.

In this section, we show that low frequency perturbations in an azimuthally rotating plasma may develop into spiral structures, which, in a particular case, are stationary. Low frequency instabilities such as the collisional drift wave instability, the centrifugal instability and the Kelvin-Helmholz instability are taken into account, and the linear eigen-value problem for the ECR plasmas is numerically solved to show the existence of spiral solutions.

The spiral structures in the gun-produced plasmas [5], in which ν_i is comparable with Ω_i, and the

ion azimuthal flow is supersonic, will be discussed separately since full nonlinear treatment is required because of no smallness parameters.

Plasmas in a cylindrical vessel are inevitably driven to rotate with the $\mathbf{E}\times\mathbf{B}$ drift due to the ambipolar potential. Then the ions are subject to centrifugal force and their rotation frequency is affected by an effective gravitational drift, while the electrons are driven by a diamagnetic drift. The difference of those velocities induce charge separation which cannot be fully cancelled by electrons whose axial motions are dragged by collisions with neutral particles. Thus fluctuations are excited and azimuthal motions are organized in such a way that the core part of the plasmas is almost rotating rigidly while the outer part lags behind the core part because the azimuthal velocities do not increase in proportion to the radius, producing a spiral structure. In the axial direction, however, the nonlinear frequency shift induced by the mode-mode coupling could be balanced with the dispersion of the modulated fluctuations, which gives localized structures of the type of an envelop soliton.

In Sec.7.1 we express the ambipolar potential in terms of the background density from the balance of the divergence of electron and ion fluxes. In Sec.7.2 we derive an equation describing fluctuations and In Sec.7.3 the localization along the magnetic fields is shown by deriving the Ginzburg and Landau equation for the modulated amplitude of the spiral. In Sec. 7.4 an eigenvalue equation in the radial direction is solved to give spiral structures which are compatible with the observations. Discussions are given in the last section.

7.1 Structure of background rotating plasmas

Equations for ions and electrons in a magnetized plasma read

$$\frac{\partial n_\alpha}{\partial t} + \nabla(n_\alpha \mathrm{v}_\alpha) = 0, \tag{7.1}$$

$$\frac{\partial \mathrm{v}_\alpha}{\partial t} + \mathrm{v}_\alpha \cdot \nabla \mathrm{v}_\alpha = \frac{e_\alpha}{m_\alpha}(-\nabla\phi + \frac{1}{c}\mathrm{v}_\alpha \times \mathrm{B}) - \delta_{\alpha,e}\frac{1}{n}\nabla p_\alpha - \nu_\alpha \mathrm{v}_\alpha. \tag{7.2}$$

where n_α, v_α and ν_α (α = e or i) are the density, velocity and collision frequency with neutral particles of electrons and ions, respectively, and ϕ is the potential.

In the following physical quantities are divided into the stationary part and fluctuating part:

$$\begin{pmatrix} n \\ \phi \\ \mathrm{v} \end{pmatrix} = \begin{pmatrix} n_0(r,z) \\ \phi_0(r,z) \\ \mathrm{v}_0(r,z) \end{pmatrix} + \sum_{\ell\neq 0}\sum_{m=1}^{\infty} \varepsilon^m \begin{pmatrix} n_\ell^{(m)}(r,\varepsilon z,\varepsilon t,\varepsilon^2 t) \\ \phi_\ell^{(m)}(r,\varepsilon z,\varepsilon t,\varepsilon^2 t) \\ \mathrm{v}_\ell^{(m)}(r,\varepsilon z,\varepsilon t,\varepsilon^2 t) \end{pmatrix} e^{i(\ell\theta + k_\ell z - \omega_\ell t)} + c.c.,$$

where ε is a smallness parameter associated with the fluctuations and is of the order of $k r_d(\nu_e/\Omega_e)$. The amplitude modulations in both t and z are due to nonlinear mode-mode couplings.

The ion drift is expressed in terms of cylindrical coordinate $\mathrm{v}_0=(u_0, v_0, w_0)$ as

$$u_{i,0} \simeq -\frac{C_s^2\nu_i}{\Omega_i^2+\nu_i^2}\frac{\partial\phi_0}{\partial r}, \tag{7.3}$$

$$v_{i,0} \simeq \frac{C_s^2\Omega_i}{\Omega_i^2+\nu_i^2}\frac{\partial\phi_0}{\partial r}\{1-(\frac{C_s\Omega_i}{\Omega_i^2+\nu_i^2})^2\frac{1}{r}\frac{\partial\phi_0}{\partial r}\}, \tag{7.4}$$

$$w_{i,0} \simeq -\frac{C_s^2}{\nu_i}\frac{\partial\phi_0}{\partial z}, \tag{7.5}$$

where $C_s^2 = T_e/M$ and $\Omega_i = eB/Mc$. The $e\phi/T_0$ has been replaced by ϕ as well. The second term of eq.(7.4) is an effective gravitational drift due to a centrifugal force. The effect of the centrifugal force on the radial drift is neglected since $\nu_i/\Omega_i << 1$. The electron drift is given in a similar way as

$$u_{e,0} \simeq \frac{v_T^2\nu_e}{\Omega_e^2+\nu_e^2}\frac{\partial}{\partial r}(\phi_0-\ln n_{e,0}), \tag{7.6}$$

$$v_{e,0} \simeq \frac{v_T^2\Omega_e}{\Omega_e^2+\nu_e^2}\frac{\partial}{\partial r}(\phi_0-\ln n_{e,0}), \tag{7.7}$$

$$w_{e,0} \simeq \frac{v_T^2}{\nu_e}\frac{\partial}{\partial z}(\phi_0-\ln n_{e,0}), \tag{7.8}$$

where $v_T^2 = T/m$ and $\Omega_e = eB/mc$. Here the diamagnetic drift is taken into account but a gravitational drift from the centrifugal force is omitted since $\nu_e/\Omega_e << 1$.

The rotation frequencies of the ion and electron azimuthal drift now read

$$\omega_0^i \simeq \omega_E(1-\frac{\omega_E}{\Omega_i}), \quad \omega_0^e \simeq \omega_E+\omega_*, \tag{7.9}$$

where ω_E and ω_* are the frequencies associated with the $\mathbf{E}\times\mathbf{B}$ drift and the diamagnetic drift, respectively, defined by

$$\omega_E = \frac{C_s^2}{\Omega_i}\frac{1}{r}\frac{d\phi_0}{dr}, \quad \omega_* = -\frac{v_T^2}{\Omega_e}\frac{1}{r}\frac{d\ln n_{e,0}}{dr}.$$

The space potential produced by the ion radial transport is short-circuited by the electron axial transport so that we have

$$\nabla(n_{i,0}\mathrm{v}_{i,0}) = \nabla(n_{e,0}\mathrm{v}_{e,0}) = Sn_{e,0}, \tag{7.10}$$

which determines the profile of the equilibrium density and potential. Since the solution of this equation is sensitively dependent on the boundary conditions at the end of the field lines unless the plasma is so long that parallel diffusion can be neglected altogether, it is unlikely to obtain a self-consistent solution $n_{i,0}(r,z)$, $n_{e,0}(r,z)$ and $\phi_0(r,z)$ to the problem of ambipolar diffusion across magnetic field. Instead, in the following we take a phenomenological approach to assume the density profiles compatible with those of laboratory plasmas and determine the potential profiles from them. Equation (7.10) is now rewritten as

$$\frac{C_s^2\nu_i}{\Omega_i^2}\frac{1}{r}\frac{\partial}{\partial r}(rn_{i,0}\frac{\partial\phi_0}{\partial r})+\frac{C_s^2}{\nu_i}\frac{\partial}{\partial z}(n_{i,0}\frac{\partial\phi_0}{\partial z}) = Sn_{e,0}, \tag{7.11}$$

$$\frac{v_T^2\nu_e}{\Omega_e^2}\frac{1}{r}\frac{\partial}{\partial r}(\xi n_{e,0}\frac{\partial}{\partial r}(\phi_0-\ln n_{e,0}))+\frac{v_T^2}{\nu_e}\frac{\partial}{\partial z}(n_{e,0}\frac{\partial}{\partial z}(\phi_0-\ln n_{e,0})) = Sn_{e,0}. \tag{7.12}$$

Invoking charge neutrality $n_{i,0} = n_{e,0} = n_0$ we have from the electron continuity equation

$$\frac{\partial}{\partial z}(n_0\frac{\partial\phi_0}{\partial z}) = \frac{\nu_e}{v_T^2}Sn_0+\frac{\partial^2 n_0}{\partial z^2}-\frac{\nu_e^2}{\Omega_e^2}\frac{1}{r}\frac{\partial}{\partial r}\{rn_0\frac{\partial}{\partial r}(\phi_0-\ln n_0)\}, \tag{7.13}$$

which is substituted into the ion continuity equation to give

$$(1-\frac{\nu_e^2}{\Omega_e^2})\frac{1}{r}\frac{d}{dr}(rn_0(r,z)\frac{d\phi_0}{dr}) = \frac{\Omega_i^2}{\nu_i^2}\{\alpha n_0 - \frac{\partial^2 n_0}{\partial z^2}\} - (\frac{\Omega_i\nu_e}{\Omega_e\nu_i})^2\frac{1}{r}\frac{\partial}{\partial r}(r\frac{\partial n_0}{\partial r}), \tag{7.14}$$

where

$$\alpha = (\frac{\nu_i}{C_s^2} - \frac{\nu_e}{v_T^2})S.$$

The profile of ϕ_0 is determined from the above equation for a given $n_0(r,z)$ as

$$\begin{aligned}\phi_0(r,z) &= -(\frac{\Omega_i\nu_e}{\Omega_e\nu_i})^2\ln n_0(r,z) \\ &\quad + \frac{\Omega_i^2}{\nu_i^2}\int_0^r dr'\frac{1}{r'n_0(r',z)}\int_0^{r'} dr''r''\{\alpha n_0(r'',z) - \frac{\partial^2 n_0(r'',z)}{\partial z^2}\},\end{aligned} \tag{7.15}$$

where we have used that $(\nu_e/\Omega_e)^2 << 1$. The ion azimuthal drift velocity is given by

$$\begin{aligned}v_{i,0} &= \frac{C_s^2}{\Omega_i}\frac{\partial\phi_0}{\partial r}(1-\frac{C_s^2}{\Omega_i^2}\frac{1}{r}\frac{d\phi_0}{dr}) \\ &\simeq -\frac{C_s^2}{\Omega_i}[(\frac{\Omega_i\nu_e}{\Omega_e\nu_i})^2\frac{d\ln n_0(r,z)}{dr} + \frac{\Omega_i^2}{\nu_i^2}\frac{1}{rn_0(r,z)}\int_0^r dr'r'\{\alpha - \frac{\partial^2}{\partial z^2}\}n_0(r',z)],\end{aligned} \tag{7.16}$$

The background density observed in the ECR plasma is a monotonically decreasing function of r and homogeneous in the axial direction, and the best-fit is given by

$$n_0(r,z) = e^{-(3/2)(r/r_d)^2},$$

which is shown in Fig.7.1(a) together with the experimental data. The ion azimuthal drift velocity obtained from this density profile through eq. (7.16) is depicted in Fig.7.1(b) where the observed ion drift velocity is represented by dots for comparison.

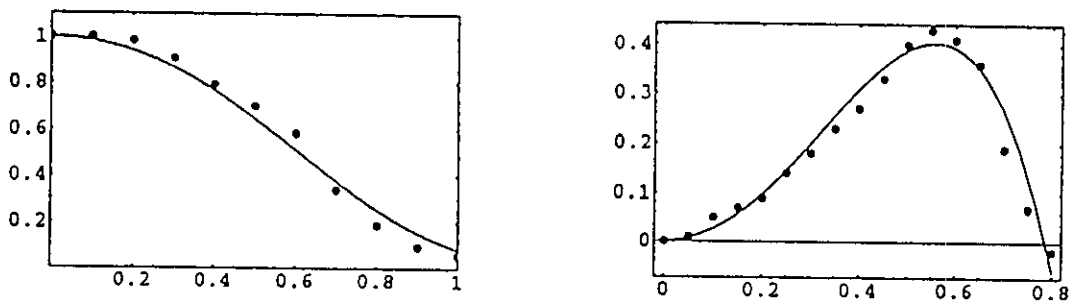

Figure 7.1: The radial profiles used in the calculations: (a) the radial profile of the density approximated by a Gaussian together with the experimental data (a dotted line) and (b)the $E\times B$ drift frequency normalized by Ω_i.

7.2 Equation for the motion of fluctuations

The first order fluctuating electron velocities given by eqs.(1) and (2) are

$$\begin{aligned} u_{e,\ell}^{(1)} &= \frac{v_T^2}{\Sigma_e(\omega_\ell)}[-\frac{i\ell(\Omega_e - 2\omega_0^e)}{r} + \Gamma_e(\omega_\ell)\frac{\partial}{\partial r}](\phi_\ell^{(1)} - \frac{n_{e,\ell}^{(1)}}{n_0}), \\ v_{e,\ell}^{(1)} &= \frac{v_T^2}{\Sigma_e(\omega_\ell)}[(\Omega_e - \omega_0^e - \frac{dv_{e,0}}{dr})\frac{\partial}{\partial r} + \frac{i\ell\Gamma_e(\omega_\ell)}{r}](\phi_\ell^{(1)} - \frac{n_{e,\ell}^{(1)}}{n_0}), \\ w_{e,\ell}^{(1)} &= \frac{v_T^2}{\Gamma_e(\omega_\ell)} ik_\ell(\phi_\ell^{(1)} - \frac{n_{e,\ell}^{(1)}}{n_0}), \end{aligned}$$

where

$$\Gamma_e(\omega) = \nu_e - i(\omega - \ell\omega_0^e), \quad \Sigma_e(\omega) = (\Omega_e - 2\omega_0^e)(\Omega_e - \omega_0^e - \frac{dv_{e,0}}{dr}) + \Gamma_e(\omega)^2.$$

Substituting these into the equation of electron continuity we have

$$\begin{aligned} [i(\omega_\ell - \ell\omega_0^e) + S]\frac{n_{e,\ell}^{(1)}}{n_0} &= v_T^2\frac{\Gamma_e(\omega_\ell)}{\Sigma_e(\omega_\ell)}\{\frac{\partial^2}{\partial r^2} + [\frac{1}{r} + (\frac{d}{dr}\ln\frac{n_0}{\Sigma_e(\omega_\ell)})]\frac{\partial}{\partial r} \\ &- [\frac{\ell^2}{r^2} + \frac{i\ell}{r}\frac{\Sigma_e(\omega_\ell)}{n_0\Gamma_e(\omega_\ell)}(\frac{d}{dr}\frac{n_0(\Omega_e - 2\omega_0^e)}{\Sigma_e(\omega_\ell)})]\}(\phi_\ell^{(1)} - \frac{n_{e,\ell}^{(1)}}{n_0}) \\ &- k_\ell^2\frac{v_T^2}{\Gamma_e(\omega_\ell)}(\phi_\ell^{(1)} - \frac{n_{e,\ell}^{(1)}}{n_0}). \end{aligned} \tag{7.17}$$

On the other hand the fluctuating parts of ion velocities are given by

$$\begin{aligned} u_{i,\ell}^{(1)} &= -\frac{C_s^2}{\Sigma_i(\omega_\ell)}[\frac{i\ell(\Omega_i + 2\omega_0^i)}{r}\phi_\ell^{(1)} + \Gamma_i(\omega_\ell)\frac{\partial\phi_\ell^{(1)}}{\partial r}], \\ v_{i,\ell}^{(1)} &= \frac{C_s^2}{\Sigma_i(\omega_\ell)}[(\Omega_i + \omega_0^i + \frac{dv_0^i}{dr})\frac{\partial\phi_\ell^{(1)}}{\partial r} - \frac{i\ell\Gamma_i(\omega_\ell)}{r}\phi_\ell^{(1)}], \\ w_{i,\ell}^{(1)} &= -\frac{C_s^2}{\Gamma_i(\omega_\ell)} ik_\ell\phi_\ell^{(1)}, \end{aligned}$$

where

$$\Gamma_i(\omega) = \nu_i - i(\omega - \ell\omega_0^i), \quad \Sigma_i(\omega) = (\Omega_i + 2\omega_0^i)(\Omega_i + \omega_0^i + \frac{dv_0^i}{dr}) + \Gamma_i(\omega)^2.$$

Substituting these into the ion continuity equation we have

$$\begin{aligned} [i(\omega_\ell - \ell\omega_0^i) + S]\frac{n_{i,\ell}^{(1)}}{n_0} &= -\frac{C_s^2\Gamma_i(\omega_\ell)}{\Sigma_i(\omega_\ell)}\{\frac{\partial^2}{\partial r^2} + [\frac{1}{r} + (\frac{d}{dr}\ln\frac{n_0}{\Sigma_i(\omega_\ell)})]\frac{\partial}{\partial r} \\ &- [\frac{\ell^2}{r^2} - \frac{i\ell}{r}\frac{\Sigma_i(\omega_\ell)}{n_0\Gamma_i(\omega_\ell)}(\frac{d}{dr}\frac{n_0(\Omega_i + 2\omega_0^i)}{\Sigma_i(\omega_\ell)})]\}\phi_\ell^{(1)} \\ &+ k_\ell^2\frac{C_s^2}{\Gamma_i(\omega_\ell)}\phi_\ell^{(1)}. \end{aligned} \tag{7.18}$$

Substituting the above velocities into the electron and ion continuity equations, invoking charge neutrality $n_{i,\ell}^{(1)} = n_{e,\ell}^{(1)} = n_\ell^{(1)}$, we have

$$\frac{d^2\phi_\ell^{(1)}}{dr^2} + [\frac{1}{r} + \frac{d\ln n_0}{dr}]\frac{d\phi_\ell^{(1)}}{dr} + [\beta(r) - \frac{\ell^2}{r^2}]\phi_\ell^{(1)} = 0, \tag{7.19}$$

where

$$\beta(r) = -\frac{k_\ell^2\Omega_e\Omega_i}{\Gamma_e(\omega_\ell)\Gamma_i(\omega_\ell)}(1-\frac{\ell\omega_*}{\omega_\ell-\ell\omega_E}) -\frac{i\ell}{r}\frac{1}{\Gamma_i(\omega_\ell)}\{(\omega_0^i+\frac{dv_0^i}{dr}+\frac{\ell\omega_E^2}{\omega_\ell-\ell\omega_E})\frac{d\ln n_0}{dr}+\frac{d\omega_0^i}{dr}+\frac{d^2v_0^i}{dr^2}\},$$

where we have neglected terms of the order of or less than $O(\Omega_i/\Omega_e)$ and $O(\omega_0^i/\Omega_i)$ and used the following approximation derived from the electron or ion continuity equation,

$$\frac{n_\ell^{(1)}}{n_0}\simeq -\frac{v_T^2}{\Omega_e^2}\frac{\ell\Omega_e}{\omega_\ell-\ell(\omega_0^e-\omega_*)}\frac{1}{r}\frac{d\ln n_0}{dr}\phi_\ell^{(1)}=\frac{\ell\omega_*}{\omega_\ell-\ell\omega_E}\phi_\ell^{(1)}. \tag{7.20}$$

Equation (7.19) describes low frequency fluctuations excited by both the collisional drift wave instability(the first term of β) and the flute mode instability such as the gravitational instability due to the centrifugal force acting on ions (the second term of β) and the Kelvin-Helmholz instability (the third and fourth terms of β). The difference between eq.(7.19) and the equation derived by Rosenbulth and Simon [6] is that the charge neutrality is assumed and the collisional drag is taken into account in eq.(7.19), while the ion diamagnetic drift is taken into account instead of the electron diamagnetic drift in Ref.[6]. Putting that $\phi_\ell^{(1)}(r,\varepsilon z,\varepsilon t,\varepsilon^2 t)=\psi_\ell(r)g_\ell(\varepsilon z,\varepsilon t,\varepsilon^2 t)/\sqrt{n_0(r)}$, eq.(7.19) is transformed to

$$\frac{d^2\psi_\ell}{dr^2}+\frac{1}{r}\frac{d\psi_\ell}{dr}+[\Lambda(r)-\frac{\ell^2}{r^2}]\psi_\ell=0, \tag{7.21}$$

where

$$\Lambda(r) = \beta(r)-\frac{1}{4}(\frac{d\ln n_0}{dr})^2-\frac{1}{2}(\frac{d}{dr}+\frac{1}{r})\frac{d\ln n_0}{dr}$$
$$\sim \begin{cases} \dfrac{-k_\ell^2\Omega_e\Omega_i}{\Gamma_e(\omega_\ell)\Gamma_i(\omega_\ell)}\dfrac{\omega_\ell-\ell\omega_0^e}{\omega_\ell-\ell\omega_E} & for\ \ k\sim 1, \\ -\dfrac{i\ell}{r}\dfrac{1}{\Gamma_i(\omega_\ell)}\{(\omega_0^i+\dfrac{dv_0^i}{dr}+\dfrac{\ell\omega_E^2}{\omega_\ell-\ell\omega_E})\dfrac{d\ln n_0}{dr}+\dfrac{d\omega_0^i}{dr}+\dfrac{d^2v_0^i}{dr^2}\} & for\ \ k\sim 0. \end{cases}$$

The ratio of the contribution from the drift wave to that from the flute mode is estimated to be $k_\ell^2(\Omega_e/\nu_e)(r_d\Omega_i/C_s)$. Therefore the collisional drift wave instability is dominant when $k_\ell^2 >> (\nu_e/\Omega_e)(C_s/r_d\Omega_i)$ is satisfied. The quantity $(\nu_e/\Omega_e)(C_s/r_d\Omega_i)$ is of the order of 10^{-4} to 10^{-5} for the laboratory plasmas and thus we only consider the cases of fluctuations due to the collisional drift wave instability:

$$\Lambda(r)\simeq\frac{k_\ell^2\Omega_e\Omega_i}{\Gamma_e(\omega_\ell)\Gamma_i(\omega_\ell)}\frac{\omega_\ell-\ell\omega_0^e}{\omega_\ell-\ell\omega_E}.$$

7.3 Localization along the magnetic field

The ion velocities in the second order of ε are dominated by convection terms and are given by

$$u_{i,\ell}^{(2)} = -\frac{C_s^4}{\Omega_i^3}\sum_{\ell'}\frac{k_{\ell'}k_{\ell-\ell'}}{\Gamma_i(\omega_{\ell'})}\phi_{\ell'}^{(1)}\frac{\partial\phi_{\ell-\ell'}^{(1)}}{\partial r}, \tag{7.22}$$

$$v_{i,\ell}^{(2)} = -i\frac{C_s^4}{r\Omega_i^3}\sum_{\ell'}\frac{(\ell-\ell')k_{\ell'}k_{\ell-\ell}}{\Gamma_i(\omega_{\ell'})}\phi_{\ell'}^{(1)}\phi_{\ell-\ell'}^{(1)}, \tag{7.23}$$

$$w_{i,\ell}^{(2)} = i\frac{k_\ell C_s^4}{\Gamma_i(\omega_\ell)}\sum_{\ell'}\frac{k_{\ell'}k_{\ell-\ell'}}{\Gamma_i(\omega_{\ell'})\Gamma_i(\omega_{\ell-\ell'})}\phi_{\ell'}^{(1)}\phi_{\ell-\ell'}^{(1)}. \tag{7.24}$$

On the other hand the electron velocities are dominated by the pressure nonlinearity in the radial and azimuthal directions and by the convection term in the axial direction. Thus we have

$$u_{e,\ell}^{(2)} = -\frac{v_T^2}{\Omega_e}\frac{\partial}{\partial r}\sum_{\ell'}\frac{\ell'(\ell-\ell')\omega_*^2}{(\omega_{\ell'}-\ell'\omega_E)(\omega_{\ell-\ell'}-(\ell-\ell')\omega_E)}\phi_{\ell'}^{(1)}\phi_{\ell-\ell'}^{(1)}, \tag{7.25}$$

$$v_{e,\ell}^{(2)} = \frac{i\ell v_T^2}{r\Omega_e}\sum_{\ell'}\frac{\ell'(\ell-\ell')\omega_*^2}{(\omega_{\ell'}-\ell'\omega_E)(\omega_{\ell-\ell'}-(\ell-\ell')\omega_E)}\phi_{\ell'}^{(1)}\phi_{\ell-\ell'}^{(1)}, \tag{7.26}$$

$$w_{e,\ell}^{(2)} = \frac{ik_\ell v_T^2}{\Gamma_e(\omega_\ell)}\sum_{\ell'}\frac{\ell'(\ell-\ell')\omega_*^2}{(\omega_{\ell'}-\ell'\omega_E)(\omega_{\ell-\ell'}-(\ell-\ell')\omega_E)}\phi_{\ell'}^{(1)}\phi_{\ell-\ell'}^{(1)}. \tag{7.27}$$

From the continuity equations for both the ions and electrons and invoking again the charge neutrality condition, we simply have

$$(\frac{\partial}{\partial t}+v_g\frac{\partial}{\partial z})g_\ell(\varepsilon z,\varepsilon t,\varepsilon^2 t)=0, \tag{7.28}$$

where

$$v_g=\frac{2\Gamma_e(\omega_\ell)\Gamma_i(\omega_\ell)}{k_\ell|\ell(\omega^{(e)}-\omega^{(i)})-i(\nu_e-\nu_i)|}.$$

From the third order equations in ε, we have

$$i\frac{\partial}{\partial t}g_\ell+p_\ell\frac{\partial^2}{\partial z^2}g_\ell+\sum_{\ell',\ell''}\frac{\psi_{\ell'}\psi_{\ell''}\psi_{\ell-\ell'-\ell''}}{\psi_\ell}V(\ell,\ell',\ell'')g_{\ell'}g_{\ell''}g_{\ell-\ell'-\ell''}=0, \tag{7.29}$$

where

$$p_\ell = -\frac{1}{2}\frac{dv_g}{dk_\ell},$$

$$V(\ell,\ell',\ell'') = \frac{p_\ell k_\ell k_{\ell-\ell'-\ell''}\ell'\ell''(\ell-\ell'-\ell'')\omega_*^3(\omega_\ell-\ell\omega_E)}{(\omega_\ell-\ell\omega_0^e)(\omega_{\ell'}-\ell'\omega_E)(\omega_{\ell''}-\ell''\omega_E)(\omega_{\ell-\ell'-\ell''}-(\ell-\ell'-\ell'')\omega_E)}.$$

Equation (7.29) is reduced to the Ginzburg-Landau equation when only the self-interaction of ℓ mode is considered:

$$i\frac{\partial}{\partial t}g_\ell+p_\ell\frac{\partial^2}{\partial z^2}g_\ell+q_\ell|g_\ell|^2g_\ell=0, \tag{7.30}$$

where

$$q_\ell=\int_0^{r_d}[V(\ell,\ell,-\ell)+V(\ell,-\ell,\ell)]|\psi_\ell(r)|^2dr.$$

Equation (7.30) is known to have a solitary wave solution [7] given by

$$g_\ell(\varepsilon z,\varepsilon t,\varepsilon^2 t)=g_0e^{-i\Psi t}[sech(Kz)]^{1+i\eta}, \tag{7.31}$$

where p_ℓ and q_ℓ are expressed as $p_\ell^{(r)}+ip_\ell^{(i)}$ and $q_\ell^{(r)}+iq_\ell^{(i)}$, and

$$\eta = -\delta+\sqrt{\delta^2+2},\quad \delta=\frac{3(p_\ell^{(r)}q_\ell^{(r)}+p_\ell^{(i)}q_\ell^{(i)})}{2(p_\ell^{(r)}q_\ell^{(i)}-p_\ell^{(i)}q_\ell^{(r)})},$$

$$|g_0|^2 = \frac{(2-\eta^2+3\eta p_\ell^{(r)})K^2}{q_\ell^{(i)}},\quad \Psi=-K^2[p_\ell^{(r)}(1-\eta^2)-2\eta p_\ell^{(i)}].$$

7.4 Radial spiral structure of fluctuations

Now the characteristic features of the spiral structures can be examined as follows. The solution is approximated in the case of weak r-dependence of the zero-th order quantities by $\psi_\ell(r) \simeq J_\ell(r\sqrt{A(r)})$, where J_ℓ is the Bessel function of the first kind. The real part of the argument of the Bessel function should be positive to give a convergent behavior while the imaginary part is responsible for a spiral structure, which comes from the imaginary part of ω_ℓ, $\Gamma_e(\omega_\ell)$ and $\Gamma_i(\omega_\ell)$. Multiplying ψ_ℓ^* to eq.(7.21) and integrating the resultant equation from the center to the edge of the plasma under the boundary condition $\psi_\ell(0) = \psi_\ell(r_d) = 0$, we have

$$\int_0^1 \xi\{|\frac{d\psi_\ell}{d\xi}|^2 + \frac{\ell^2}{\xi^2}|\psi_\ell|^2 - A(\xi)|\psi_\ell|^2\}d\xi = 0, \tag{7.32}$$

where r is normalized as $\xi = r/r_d$. From the imaginary part of this equation we have

$$\int \Im A(\xi)\xi|\psi_\ell(\xi)|^2 d\xi = 0,$$

which corresponds to the Rayleigh condition. For a collisional drift mode, we have at the marginal instability ($\gamma \sim 0$)

$$\Im A(\xi) = \frac{\nu_e k^2 \Omega_e \Omega_i(\omega_r - \ell\omega_0^e)(\omega_r - \ell\omega_0^i)(\omega_r - \ell\omega_E)}{|\Gamma_e(\omega)|^2|\Gamma_i(\omega)|^2[(\omega_r - \ell\omega_E)^2 + \gamma^2]},$$

from which the Rayleigh condition holds even when $\omega_r = 0$, indicating the formation of stationary spiral structures. The winding direction of spiral arms is reversed when the magnetic fields is changed in sign since the imaginary part of $A(\xi)$ is proportional to the odd power of the magnetic field for $\omega_r = 0$. Certainly rotating spirals exist as well.

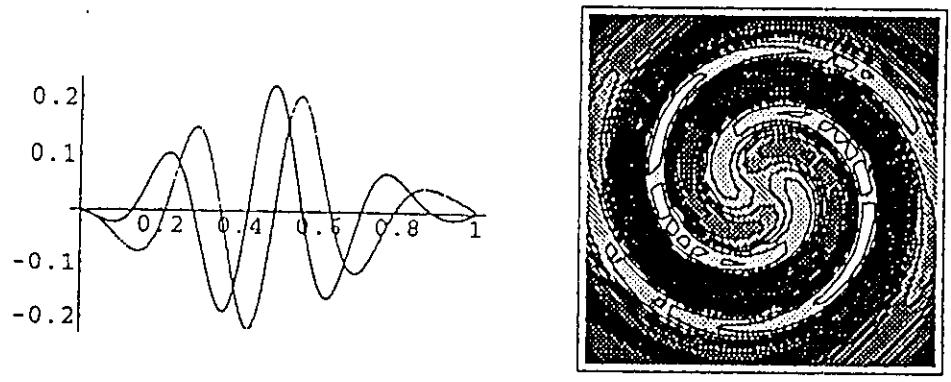

Figure 7.2: The numerical results for a stationary spiral solution for $M/m = 80000, k = 0.0225, \gamma/\Omega_i = 0.024$: (a) the radial profile of the potential: a solid line is the real part, and dotted line the imaginary part. (b) the density perturbation contour.

Here we solve eq.(7.19) numerically with the boundary condition $\psi_\ell(0) = \psi_\ell(1) = 0$. We have both stationary ($\omega_r = 0$) and rotating ($\omega_r \neq 0$) spiral solutions for a given profile of the density and the potential. The numerical results for the stationary solution are shown in Fig.7.2, where Fig.7.2(a)

is the radial potential profile (eigen function), and Fig.7.2(b) the density perturbation contour calculated by eq.(7.20). The spiral structure is identified with the Archimedes spiral, which is seen from an eikonal approximation for the solution of eq.(7.19), in the case of weak ξ-dependence of $\beta(\xi)$, that is, $\psi_l(\xi)\exp[il\theta] \sim \exp[i\int \Im[\sqrt{\beta}]d\xi + il\theta) \sim exp(i\Im\{\sqrt{\beta(\xi)}\}\xi + il\theta)$ for $\xi \neq 0$. The contour structure is similar to the observed spiral.

The vector field plot of the ion velocity field associated with the spiral structure exhibits the similar spiral structure, which well explained by the $\mathbf{E} \times \mathbf{B}$ drift due to the perturbed potential ϕ_l. It should be noted that the pattern of the perturbed flow associated with this spiral indicates a material circulation between the core and peripheral regions.

The imaginary part of the eigenvalue γ decreases with an azimuthal mode number l, which corresponds to the fact that the observed stationary spiral are always with two arms.

Even when we neglect the contributions from the centrifugal and the Kelvin-Helmholz instabilities, there is no change in this pattern. Thus, the spiral structure for this choice of parameters is identified due to the collisional drift wave instability.

In the above we have used a special profile for the density and potential since we need to compare numerical spiral structures with those observed in Ref.[4]. However, the spiral solutions of eq.(7.19) have been checked insensitive to the spatial profiles of ω_E.

For different parameters granulated density structures are obtained, which is regarded as formation of vortex crystallization. Although the vortex crystallization has been reported to be experimentally observed in pure electron plasmas [2], this type of structures may be general entities excited in magnetized plasmas.

7.5 Discussion

Formation of spiral structures is a rather general characteristic in magnetized rotating plasmas since the energy stored in a form of plasma inhomogeniety such as density and velocity shear is released to give an instability which causes a phase difference between the real and imaginary parts of eigen-functions, driving a spiral structure. Instabilities could be the collisional drift wave instability, centrifugal instability, and Kelvin-Helmholz instability, although the collisional drift wave instability is dominant for ordinary laboratory plasmas. Even in stable cases, collision plays the same role as instabilities in producing phase difference between the real and imaginary parts of the eigen-function. Therefore collision is also essential to the formation of spiral structures. Under the special condition that the potential is such that ω_E becomes zero somewhere in the radial direction within the plasma, the stationary spiral structure becomes similar to those observed in the experiment. For a wide variety of density and potential profiles rotating spiral structures are normally excited.

We have obtained linear eigen-functions to show the spiral structure formations in magnetized rotating

plasmas. The next step is to study the nonlinear stage of evolution and show why spiral structures are so robust. We are also planning to develop our theory to understand the formation of spiral structures observed in a gun-produced plasma [5]. It is worth noting that our study may contribute to understanding the mechanism of spiral galaxy formation.

References

[1] M.V.Nezlin and E.N.Snezhkin, *Rossby Vortices, Spiral Structures, Solitons*,(Springer-Verlag, Berlin,1993)

[2] K.S.Fine, A.C.Case, W.G.Flynn and C.F.Driscoll, Phys. Rev. Lett. **75**, 3277 (1995)

[3] Y.Amagishi, Y.Yoshikawa and J.Ohara, J.Phys.Soc.Jpn **60**, 2496 (1992)

[4] M.Y.Tanaka, T.Sakamoto, H.Imaizumi, K.Taniguchi and Y.Kawai, Proc. 1996 Int. Conf. on Plasma Physics(Nagoya, Japan) Vol.2, 1650 (1997)

[5] T.Ikehata, H.Tanaka, N.Y.Sato and H.Mase, Phys. Rev. Lett. **81**, 1853 (1998)

[6] M.N.Rosenbulth and A.Simon, Phys. Fluids **8**, 1300 (1965)

[7] K. Nozaki and N. Bekki, J. Phys. Soc. Jpn. **53**, 1581 (1984)